17th World Conference on Earthquake Engineering, 17WCEE
Sendai, Japan - September 13th to 18th 2020

SEISMIC PERFORMANCE OF BRACED FRAMES CONSIDERING FRACTURE AND LOCAL BUCKLING OF MEMBERS

R. Matsui[(1)], J. Ariga[(2)], T. Takeuchi[(3)]

[(1)] *Associate professor, Hokkaido University, ryota.matsui@eng.hokudai.ac.jp*
[(2)] *Graduate student, Tokyo Institute of Technology, e-mail address*
[(3)] *Professor, Tokyo Institute of Technology, e-mail address*

Abstract

One of the key states governing the ultimate seismic performance of steel structures is sidesway collapse. For the numerical investigation on the sideway collapse, deterioration associated with flexural buckling, local buckling or fracture of steel members is essential. Past studies developed numerical models to capture this deterioration for structures. Those numerical models for steel structures are basically divided into three difference categories: the phenomenological model (PM), the physical theory model (PTM) and the continuum finite element model (CFEM). The advantage of PMs is accurate because the hysteresis is constituted based on observed experimental data. The constitutive rule of PTMs is constructed based on common material properties or dimension properties. Compared to the PM and PTM, the CFEM is more sophisticated approach to obtain deterioration behavior. The CFEM accurately reproduced the degradation of force-displacement relation due to local buckling deformation and longitudinal plastic strain distribution of steel components subjected to cyclic loading. This paper represents a short literature review of the recent deterioration models for steel structures proposed by the Japanese researchers. Subsequently, a displacement-based fiber element incorporating softening accounting for the local buckling of I-shaped section columns subjected to axial and lateral loads based on a physical theory was introduced. This was followed by a discussion of comparison to the results of the 2D-element CFEM simulation. This physical fiber element was implemented in framework system of in-house program for incremental dynamic analysis to capture the effect of the local buckling-induced softening for seismic performance of the braced frame.

Keywords: Deterioration model: Fracture analysis; Local buckling; I-shaped section columns; Braced frame.

1. Introduction

One of major objectives for scientific research of steel structures is prevention of sidesway collapse in the seismic standpoint. [1, 2] To address sidesway collapse, guidelines for seismic design of buildings [e.g. 3] depend heaviliy on accuracy of simulation of earthquake-induced response. Deterioration models of steel components of force-displacement relation are essential. [4] Past studies developed deterioration models for numerical simulation of versatile structures. [5, 6]. According to D'Aniello et al. [7], the deterioration models for steel structures were basically divided into three difference categories: the phenomenological model (PM), the physical theory model (PTM) and the continuum finite element model (CFEM).

The constitutive rule of PMs is simplified based on observed experimental data. Although the advantage of the PM is simulating response accurately, this model requires results of individual physical tests. The constitutive rule of PTMs is constructed based on common material properties or dimension properties presented a PTM to fairly predict the force-displacement relation of circular hollow section beam. Compared to the PM and PTM, the CFEM is more sophisticated approach to obtain response of large inelastic behavior. The CFEM accurately reproduces the degradation of moment-rotation relation, axial shortening due to local buckling deformation and longitudinal plastic strain distribution of steel components subjected to cyclic loading based on one- (1D), two- (2D) or three-dimensional (3D) elements.

This paper by describing a short literature review of several recent deterioration models using the PM or PTM for steel structures proposed by the Japanese researchers. Subsequently, a displacement-based fiber

element incorporating a constitutive hysteresis model accounting for the local buckling-induced softening of I-shaped section columns subjected to axial and lateral loads [8] based on a physical theory [9] was introduced. Hence forth this element is referred to as the "physical fiber element". This was followed by a discussion of comparison to the results of the 2D-element CFEM simulation. This physical fiber element was implemented in framework system of in-house program for incremental dynamic analysis to capture the effect of the local buckling-induced softening for seismic performance of a braced frame.

2. Literature review of recent deterioration models in Japan

The following descriptions shortly lists the literature review of deterioration models using the PM or PTM of the recent studies on steel structure in Japan.

One of the most general PM is the Shibata-Wakabayashi model for steel braces [10] in Japan. Four functions were used for the constitutive model for the hysteresis rule of Shibata-Wakabayashi model (SW model). Shimizu et al. [11] indicated the SW model [10] agreed in the strength of slender steel braces compared with the PM proposed by Kato [12]. Some researchers modified the SW model to capture more accurate hysteresis of the steel braces. Taniguchi et al. [13] incorporated the peak strength in compression side into the SW model. Ito et al. [14] reviewed the parameters of the SW model with past structural tests. Hashimoto et al. [15] proposed an alternative coefficient for the flexural buckling-induced softening based on 100 samples of physical tests. Idota et al. [16] developed a PM for steel beams to capture the lateral buckling-induced softening. As far as the authors know, the limited number of PTMs was developed in recent years in Japan.

3. Formulation of physical fiber element for rectangular hollow section columns

Physical fiber elements were formulated using several subdivisions in a basic system, as shown in Fig. 1. Fibers were used for the section of the physical fiber element to capture the plasticity of the flanges and web. For formulation of the physical fiber element, those flanges and web were referred to "plate". Gauss-lobatto quandrature was used in subdivisions to express the inelastic force and deformation of sections at the element ends. The material strain of each fiber was defined by the section deformations using the Euler-Bernoulli hypothesis

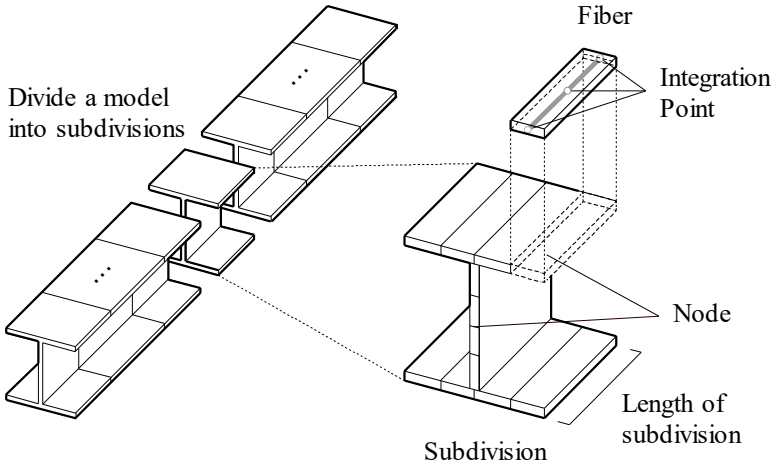

Fig. 1 – Modeling of physical fiber element

3.1 Constitutive model for restoring-force-hysteresis

The stress-strain relation of the fiber was decomposed into six stages based on the phenomenological model [8], to incorporate strain hardening and softening as Eq. (6.1):

$$n=\begin{cases}\alpha & \left(Stage\ A\ :\delta_a\le\delta\right)\\ n_r+\dfrac{\delta-\delta_r}{e_t} & \left(Stage\ A'\ :\delta_r\le\delta<\delta_a\right)\\ n_p+\dfrac{n_r-n_p}{\delta_r-\delta_p}\left(\delta-\delta_p\right) & \left(Stage\ B\ :\delta_p\le\delta<\delta_r\right)\\ f_c\quad\text{(Eq.(23))} & \left(Stage\ C\ :\delta\le\delta_b\right)\\ n_b+\dfrac{\delta-\delta_b}{e_t} & \left(Stage\ C'\ :\delta_b<\delta\le\delta_q\right)\\ n_q+\dfrac{n_p-n_q}{\delta_p-\delta_q}\left(\delta-\delta_q\right) & \left(Stage\ D\ :\delta_q<\delta\le\delta_p\right)\end{cases} \tag{1}$$

where, n = the normalized-force; δ = the normalized-deformation; κ = the coefficient derived from failure mechanism; α = the ultimate tensile normalized-force; e_t (= E / E_t) = the inverse of the strain hardening ratio, where E was the elastic modulus and E_t was the inelastic tangent modulus; t = the thickness of the section; and B = the width of the section in the following chapter. The normalized-force, n, was the stress of the fiber, σ, divided by the yield strength, σ_y. The normalized-deformation, δ, was the deformation of the fiber divided by the yield strain, ε_y (= σ_y / E). Subscripts of the normalized force and deformation expressed values at the thresholds a, b, p, q and r respectively, as shown in Fig. 2. The local buckling stress, f_c , was defined in Eq. (23).

For compression side, the normalized-force, n_0, at the initiation of local buckling, was computed based on Eq. (2) of the critical load of a uniaxially compressed plate, σ_{cr} as follows:

$$\sigma_{cr}=k\frac{\pi^2E}{12\left(1-\nu^2\right)}\left(\frac{t}{B}\right)^2 \tag{2}$$

where, k = the coefficient depends on the boundary condition of the plate; and ν = the Poisson's ratio. Eqs. (3) and (4) were used to extend the normalized-force, n_0, to the inelastic range based on the column curve.

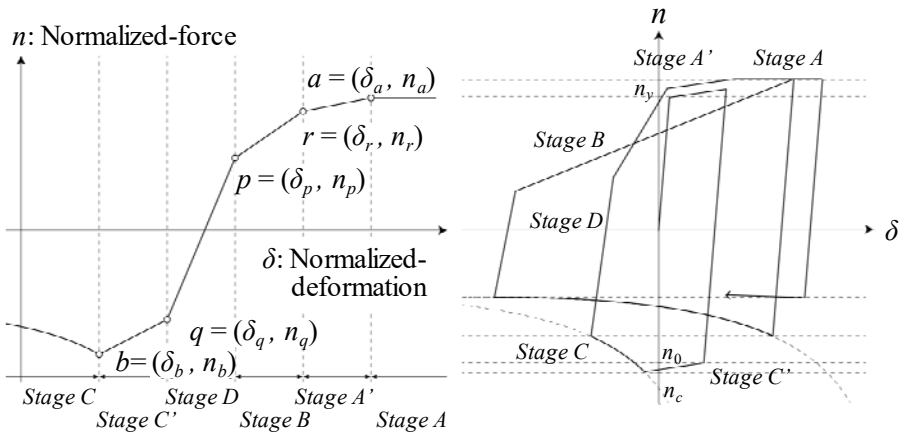

Fig. 2 – Schematic of restoring-force-hysteresis for fibers

$$\lambda_c = \sqrt{\frac{\sigma_y}{\sigma_{cr}}} \tag{3}$$

$$n_0 = \frac{\sigma_0}{\sigma_y} = \begin{cases} 1 & \lambda_c \le 1 \\ \dfrac{1}{\lambda_c^2} & 1 < \lambda_c \end{cases} \tag{4}$$

The normalized-force, n_c, at the initiation of local-buckling induced softening was determined as the intersect between the function of *Stage C* and *Stage C'*.

3.2 Algorithm for thresholds of restoring-force-hysteresis

The following description is the algorithm for thresholds for restoring-force hysteresis of the physical fiber element. The normalized-force and the normalized-deformation at the thresholds as shown in Fig. 2 on the initial condition were summarized in Eq. (5).

$$\begin{cases} n_a = \alpha & \delta_a = 1.0 + e_t\left(\alpha - 1.0\right) \\ n_p = n_r = 1.0 & \delta_p = \delta_r = 1.0 \\ n_q = -n_0 & \delta_q = -n_0 \\ n_b = -n_c & \delta_b = \delta_q - e_t\left(n_c - n_0\right) \end{cases} \tag{5}$$

The increments of normalized-deformation, δ', and normalized-force, n', in compression side were assumed to be half of those in tension side as Eq. (6):

$$\begin{cases} \delta_t^{'} = \delta_c^{'} \\ n_t^{'} = 0.5 n_c^{'} \end{cases} \tag{6}$$

Except for *Stage D*, the thresholds were updated as Eqs. (7) – (11).

For $\delta < \delta_{pre,\,b}$ (*Stage C*):

$$\begin{cases} n_{sub,q} = n \qquad \delta_{sub,q} = \delta \\ \delta_{sub,a} = \delta_{pre,a} - \left(\delta_{pre,q} - \delta_{pre,b}\right) \le \delta_{old\,a} \\ \delta_{sub,r} = \delta_{pre,r} - \left(\delta_{pre,q} - \delta_{pre,b}\right) \le \delta_{old\,r} \\ n_{sub,p} = n_{sub,r} - \left(n - n_c\right) \; \delta_{sub,p} = \delta_{sub,r} - \left(\delta_{pre,b} - \delta\right) \end{cases} \tag{7}$$

For $\delta_{pre,\,b} \le \delta < \delta_{pre,\,q}$ (*Stage C'*):

$$\begin{cases} n_{sub,q} = n\delta_{sub,q} = \delta\delta_{sub,a} = \delta_{pre,a} - \left(\delta_{pre,q} - \delta\right) \\ \delta_{sub,p} = \delta_{pre,p} - \left(\delta_{pre,q} - \delta\right) \qquad \delta_{sub,r} = \delta_{pre,r} - \left(\delta_{pre,q} - \delta\right) \end{cases} \tag{8}$$

For $\delta_{pre,\,p} \le \delta < \delta_{pre,\,r}$ (*Stage B*):

$$\begin{cases} n_{sub,p} = n \qquad \delta_{sub,p} = \delta \\ \delta_{sub,q} = \delta_{pre,q} + \left(\delta - \delta_{pre,p}\right) \qquad \delta_{sub,b} = \delta_{sub,q} - \left(\delta_{pre,q} - \delta_{pre,b}\right) \end{cases} \tag{9}$$

For $\delta_{pre,\,r} \le \delta < \delta_{pre,\,a}$ (*Stage A'*):

$$\begin{cases} n_{sub,p} = n_{sub,r} = n\delta_{sub,p} = \delta_{sub,r} = \delta \\ \delta_{sub,q} = \delta - \left(n + n_{pre,q}\right) \;\; \delta_{sub,b} = \delta_{sub,q} - \left(\delta_{pre,q} - \delta_{pre,b}\right) \end{cases} \tag{10}$$

For $\delta_{pre,\,a} \le \delta$ (*Stage A'*):

$$\begin{cases} n_{sub,a} = n_{sub,p} = n_{sub,r} = n \qquad \delta_{sub,a} = \delta_{sub,p} = \delta_{sub,r} = \delta \\ \delta_{sub,q} = \delta - \left(n + n_{pre,q}\right) \;\; \delta_{sub,b} = \delta_{sub,q} - \left(\delta_{pre,q} - \delta_{pre,b}\right) \end{cases} \tag{11}$$

3.3 Geometry modeling of collapse of plate for local-buckling induced softening

The key parameter of the proposed element was the local buckling stress, f_c. In this paper, this value was defined from energy equilibrium presented by Kato [9]. Fig. 3 illustrates the geometry modeling of collapse mechanism of the flange and web in an I-shaped section. The maximum bending moment of the plate subjected to axial load per unit length was calculated as follows:

$$M = \frac{\sigma_y}{4} t^2 \mu \tag{12}$$

$$\begin{cases} \mu = \dfrac{\beta^2 - \left(2\sin^2\phi - \cos^2\phi\right)^2}{2\beta} \\ \beta = \sqrt{\cos^4\phi + 4\left(\alpha^2 - \cos^2\phi\left(1 + 2\sin^2\phi\right)\right)} \end{cases} \tag{13}$$

where ϕ = the angle between the axial load and yielding lines as shown in Figs. 3(d) and (e). The work of the plate done by the axial load, T, was calculated as follows:

$$T = 2Bt\Delta\sigma \tag{14}$$

where B = the width of the plate; Δ = the deformation in the compression side; and σ = the longitudinal stress generated by the axial load. The energy of the yield lines done by the shear was calculated as follows:

$$U_s = \tau \frac{2\Delta}{\cos\phi} \frac{B_f}{2\sin\phi} t = \sigma_y \sin\phi\cos\phi \frac{\Delta}{\cos\phi} \frac{B_f}{\sin\phi} t = B_f t_f \Delta\sigma_y \tag{16}$$

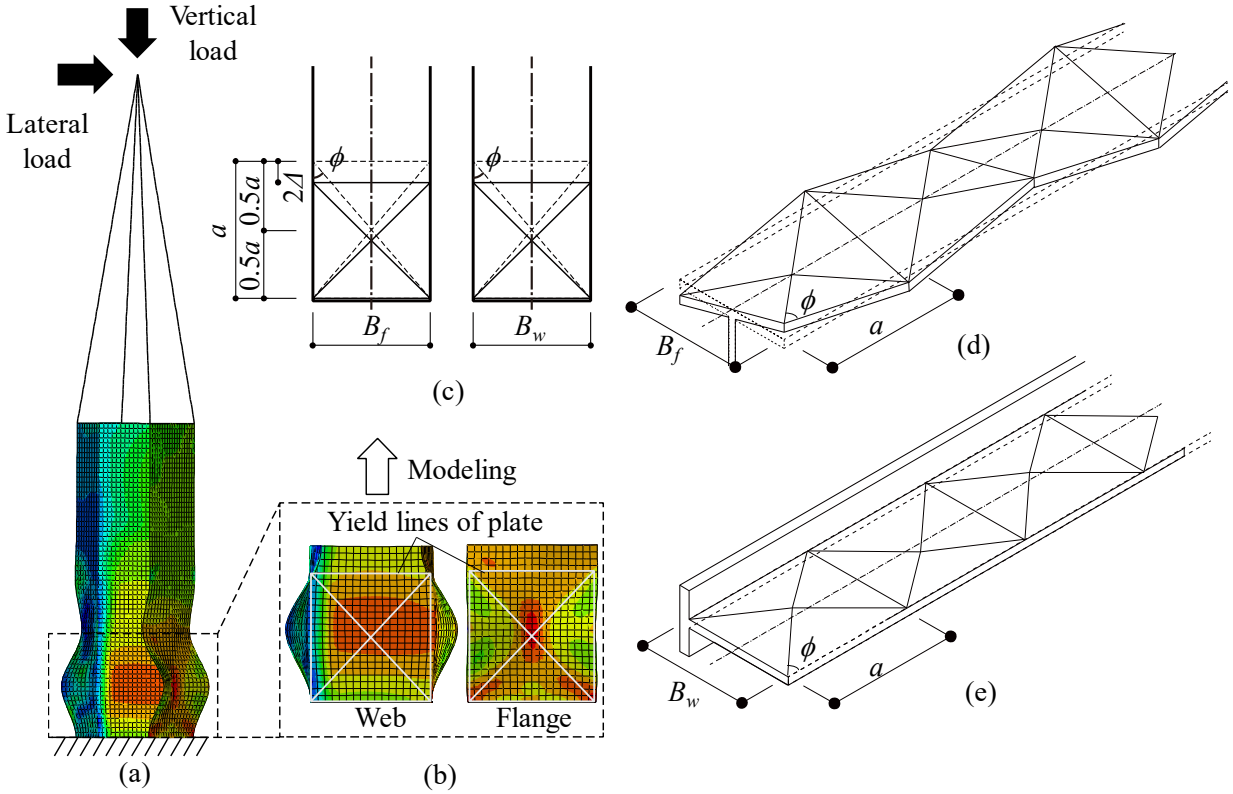

Fig. 3 – Geometry modeling of local buckling-induced deformation for rectangular hollow sections:
(a) Deformation of a cantilevered column subjected to horizontal and vertical force; (b) Assumption of yield lines; (c) Geometry modeling of local buckling-induced deformation of plate; (d) 3D geometry modeling for flange; and (e) 3D geometry modeling for web.

The energy of the yield lines done by the flexure was calculated as follows:

$$U_b = M\frac{2\sqrt{a\Delta}}{a\sin\phi}\frac{2B_f}{\sin\phi} = \frac{\sqrt{a\Delta}}{a\sin\phi}\frac{B_f}{\sin\phi}\mu {t_f}^2\sigma_y \tag{17}$$

The sum of energy done by internal force was equal to the work done by external force as follows:

$$\begin{cases} T = U_s + U_b \\ 2B_f t_f \Delta\sigma = B_f t_f \Delta\sigma_y + \dfrac{\sqrt{a\Delta}}{a\sin\phi}\dfrac{B_f}{\sin\phi}\mu {t_f}^2\sigma_y \end{cases} \tag{18}$$

The axial stress, σ, was calculated as follows:

$$\sigma = \frac{1}{2}\sigma_y + \frac{1}{\sqrt{2}\cos\phi\sin\phi}\sqrt{\frac{a}{2\Delta}}\mu\frac{t_f}{B_f}\sigma_y \tag{19}$$

It is noted that the stress, σ, was absolute. The normalized-force, n, was calculated as follows:

$$n = -\frac{\sigma}{\sigma_y} = -\frac{1}{2}\sigma_y - \frac{1}{\sqrt{2}\sin\phi\sin\phi}\sqrt{\frac{a}{2\Delta}}\mu\frac{t_f}{B_f}\sigma_y \tag{20}$$

Here, the strain of the plate as shown in Fig. 3(b), ε, was calculated as follows:

$$\varepsilon = \frac{2\Delta}{a} \tag{21}$$

The strain, ε, could be written as a function of the normalized-deformation as follows:

$$\varepsilon = \left(\delta_b + \delta_c - \delta\right)\varepsilon_y \tag{22}$$

The strength in compression side, f_c, was expressed as the normalized-deformation as follows:

$$f_c = -\frac{1}{2} - \kappa\sqrt{\frac{1}{\left(\delta_b + \delta_c - \delta\right)\varepsilon_y}}\frac{t_f}{B_f} \tag{23}$$

$$\kappa = \frac{\left(\mu + 3\mu\sin^2\phi\right)}{\sqrt{2}\sin\phi\cos\phi} \tag{24}$$

The normalized-force, n_c, at the initiation of local-buckling induced softening was calculated as the solution of the cubic function Eq. (25):

$$\begin{cases} n_c\left(n_c - 0.5\right)^2 = \left(\kappa\dfrac{t}{B}\right)^2\dfrac{1}{\varepsilon_y} \\ \left(\left(n_c - n_0\right)\dfrac{E}{E_t} + n_0\right)\left(n_c - 0.5\right)^2 = \left(\kappa\dfrac{t}{B}\right)^2\dfrac{1}{\varepsilon_y} \end{cases} \tag{25}$$

Takeuchi et al. [8] conducted the continuum finite element simulation of benchmark specimens to determine the angle, ϕ, for the yield lines as 45 deg., and the length of local buckling, a, as the width of the plate B.

4. Validation of physical fiber element compared with physical tests

Matsui et al. [17] proposed a condition for the minimum division of the physical fiber element to decrease trivial division-dependence as shonw in Fig. 4. The minimum length of the subdivision was identical with the length of the local buckling-induced half wavelength l_p, which is identical with the width of the flange. Division of the physical fiber element was determined based on the ratio of the total length of

the

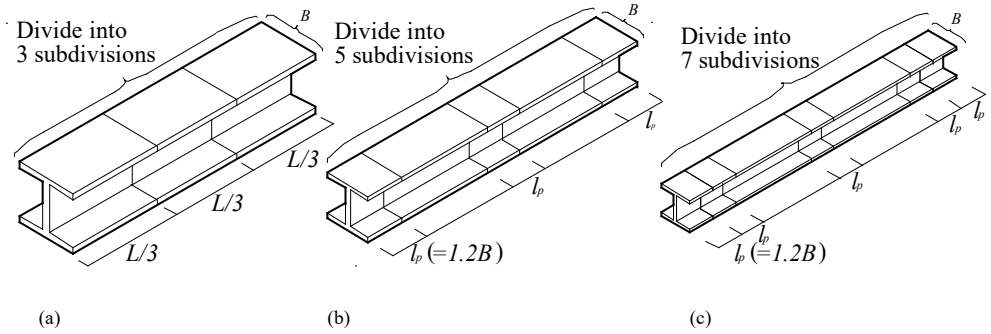

Fig. 4 –Division of physical fiber element for I-shaped section column: (a) For 3-subdivision; (b) For 5-subdivision; and (c) For 7-subdivision.

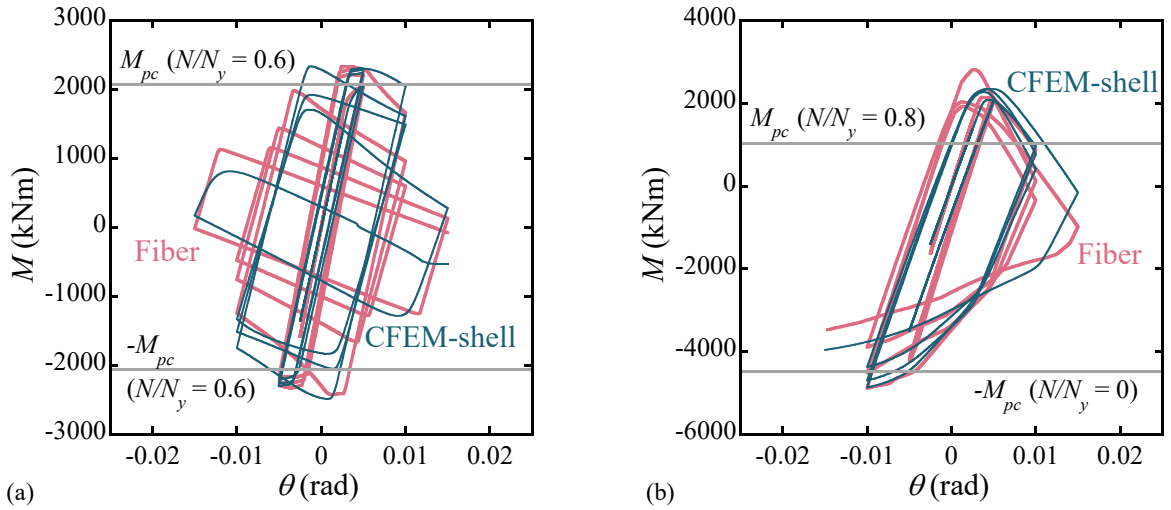

Fig. 5 –Physical fiber element versus CFEM-shell element moment-rotation curve about major-axis for I-shaped column measures 4000 mm long, 700 mm wide and 700 mm deep:

(a) $B/2t$ = 14.0, Axial load ratio N/N_y = 0.6, Constant; and (b) $B/2t$ = 14.0, $-0.8 \leqq N/N_y \leqq 0$, Variable.

column to the width of the flange by Eq. (27)

$$\begin{cases} 3-\text{subdivision} & \left(L/B \le 3.6\right) \\ 5-\text{subdivision} & \left(3.6 \le L/B \le 10.8\right) \\ 7-\text{subdivision} & \left(10.8 \le L/B\right) \end{cases} \tag{26}$$

Fig. 5 compares the moment-rotation about major axis calculated by the physical fiber element versus the CFEM-shell for a I-shaped section column. The I-shaped column measured 4000 mm long, 700 mm wide and 700 mm deep, subjected to constant or variable axial load. The response by the physical fiber element fairly captured the local buckling-induced softening of that by the CFEM-shell element. Takeuchi et al. [8] and Matsui et al. [17] validated this trend for the following data sets:

1. The depth of the I-shaped sections was mainly identical with the width.

2. The depth of the I-shaped sections subjected to axial load ranged from 72 mm to 120 mm.
3. The depth of the I-shaped sections subjected to axial load and shear measured 700 mm. The loading protocol for axial load is constant or variable.

5. Utilization of physical fiber element for collapse analysis

Fig. 6 represents model properties of a braced frame based on a fuel power plant. The figure shows the dimension properties, and stress-strain hysteresis rules for elements. Table 1 represents the dimension properties, material properties, settings for weight, and configurations of numerical models for elements. The braced frame measured 40 m wide, and 72.6 high. The depth of columns ranged from 500 mm to 1500 mm, the depth of beams ranged from 600 mm to 2,100 mm, and the diameter of braces ranged from 346 mm to 749 mm. The bilinear model, the modified SW model [13], and the softening model constituted by the physical fiber elements were used for each element of Model A and B as listed in Table 1(d). The subdivision for the columns and beams of Model A was determined by Eq. (26). According to the study [18], strain concentration ratio was used for evaluation of fracture of the brace members. After the brace members fracture, the stiffness of the braces was reduced to 0.1% times that in elastic-plastic state, as well as the strength was reduced to zero. Fig. 7 illustrates the acceleration spectrum of the input ground motion. The scale factor of the input ground motion was 1.0, which is a standard level in the Japanese seismic design. The time interval was 0.01 s. The Newmark-β method was used for the collapse analysis. Coeffiecient β was 0.25. The Rayleigh damping was used, and both damping ratios of 1st and 2nd mode were 0.05.

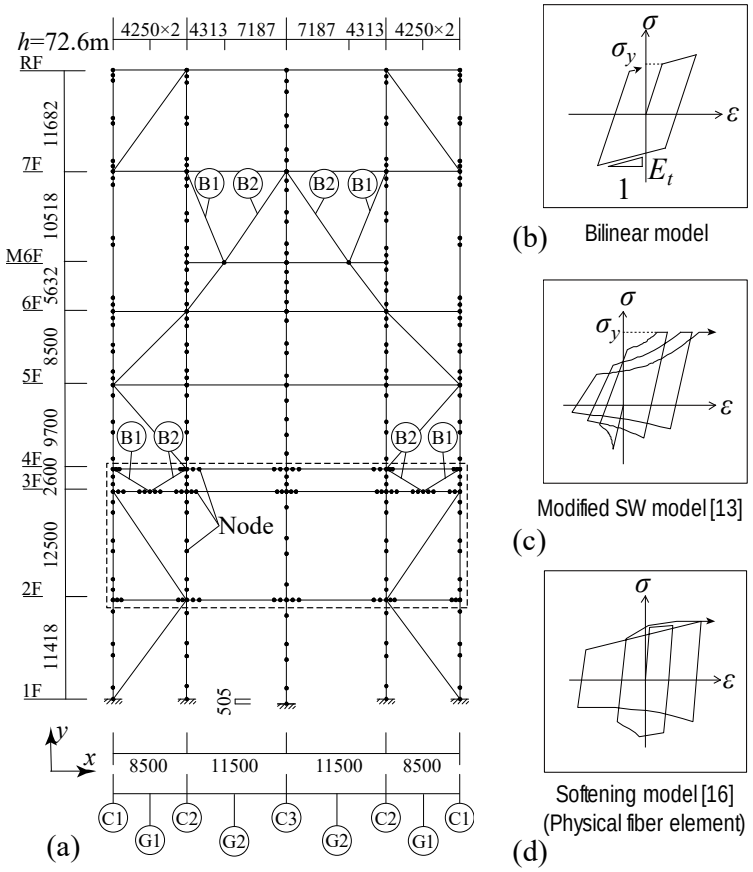

Fig. 6 – Model properties of braced frame: (a) Dimension properties; (b) Stress-strain curve of bilinear model; (c) Stress-strain curve of modified SW model; and (d) Stress-strain curve of softening model.

Table 1 – Dimension and material properties of braced frame: (a) Dimension properties; (b) Material properties; (c) Total and distribution of weight; and (d) Configuration of numerical models for elements

Dimension properties

	Columns	Beams	Brace
7F	C1: H-500 x 500 x 12 x 16 C2: H-500 x 500 x 14 x 19 C3: H-1050 x 1050 x 25 x 36	G1: H-700 x 350 x 12 x 25 G2: H-2100 x 500 x 28 x 60	B1: ϕ – 519 x 21 B2: ϕ – 519 x 21
6F	C1: H-650 x 650 x 14 x 22 C2: H-700 x 700 x 16 x 25 C3: H-900 x 900 x 22 x 32	G1: H-700 x 450 x 12 x 40 G2: H-700 x 500 x 12 x 40 G2: H-600 x 300 x 22 x 25 (M6F)	B1: ϕ – 506 x 15 B2: ϕ – 691 x 31
5F		G1: H-700 x 450 x 12 x 40 G2: H-700 x 500 x 12 x 40 G2: H-600 x 300 x 22 x 25 (M6F)	B1: ϕ – 692 x 28 B2: ϕ – 692 x 28
4F	C1: H-1000 x 1000 x 22 x 36 C2: H-1000 x 1000 x 22 x 36 C3: H-1500 x 1500 x 32 x 50	G1: H-800 x 450 x 12 x 36 (4F) G2: H-800 x 450 x 22 x 40 (4F) G1: H-900 x 300 x 14 x 33 (3F) G2: H-1500 x 600 x 16 x 40 (3F)	B1: ϕ – 749 x 27 (4F) B2: ϕ – 749 x 27 (4F) B1: ϕ – 346 x 15 (3F) B2: ϕ – 346 x 15 (3F)
3F			
2F		G1: H-600 x 500 x 12 x 18 G2: H-800 x 450 x 22 x 40	B1: ϕ – 490 x 25 B2: ϕ – 490 x 25
1F	C1: H-1100 x 1100 x 25 x 40 C2: H-1250 x 1250 x 30 x 45 C3: H-1500 x 1500 x 32 x 50	G1: H-1000 x 400 x 16 x 40 G2: H-1200 x 600 x 16 x 40	B1: ϕ – 445 x 23 B2: ϕ – 445 x 23

Description rule:
H-Depth x Width x Thick. of web x Thick. of flange for I-shaped section.
ϕ – Diameter x Thickness for Circular hollow sections.

(a)

Material properties

Model	E (N/mm²)	E_t (N/mm²)	σ_y (N/mm²)
Column	205,000	2,050	400
Beam ($t \leqq 40$ mm)	205,000	2,050	325
Beam (40 mm < t)	205,000	2,050	295
Brace	205,000	-	325

(b)

Total and distribution of weight

	2F	3F	4F	5F	6F	M6F	7F	RF
Vertical (%)	9.8	5.5	24.7	6.2	5.0	3.3	17.9	27.5
Total of vertical weight: 52,583 kN								
Horizontal (%)	14.4	11.7	8.4	20.9	18.5	5.1	14.8	6.1
Total of horizontal weight: 64,407 kN								

(c)

Configuration of numerical models for elements

Model	Floor	Columns	Beams	Braces
A	4F – 7F	Bilinear	Bilinear	Modified SW
	1F – 3F	Bilinear	Bilinear	Modified SW
B	4F – 7F	Softening	Bilinear	Modified SW
	1F – 3F	Softening	Softening	Modified SW

(d)

Fig. 8 compares the simulated results of Model A versus Model B based on the incremental dynamic analysis. The story drift angle of Model B was significantly larger than that of Model A as the scale factor increases from 3.0. This indicates the local buckling-induced softening had effect on the time-history numerical simulation results when the scale factor of the ground motion was larger than 3.0.

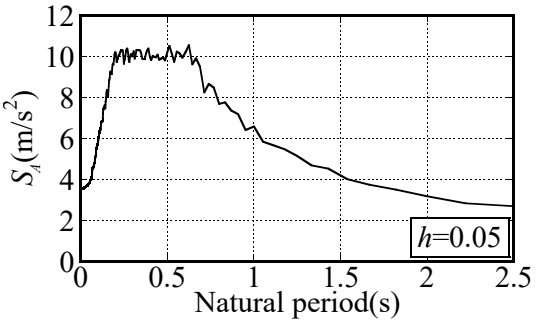

Fig. 7 – Acceleration spectrum of input ground motion (Scale factor = 1.0).

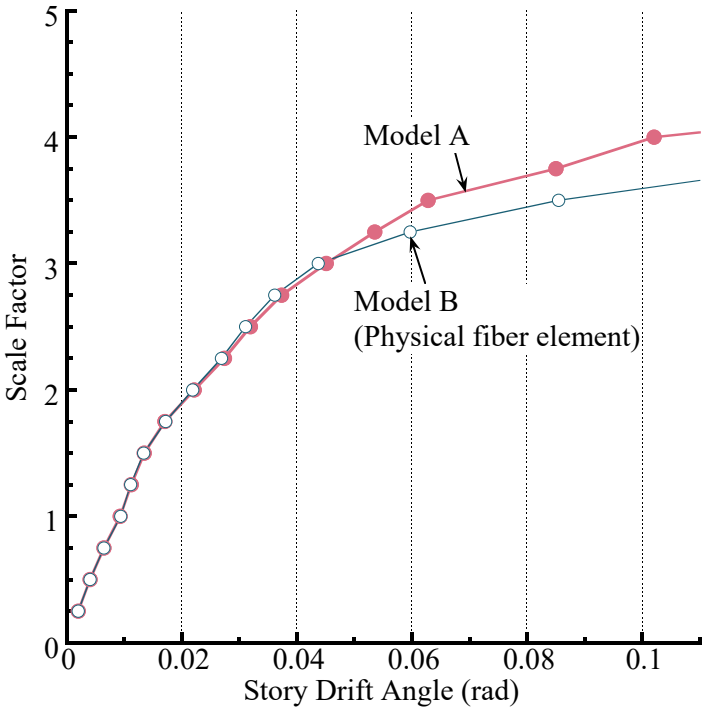

Fig. 8 –Implementation of physical fiber element for incremental dynamic analysis of braced frame.

6. Conclusions

This paper presents the literature review of the deterioration models for the elements of steel structures in the recent Japanese society. The constitutive model, algorithm, and validation of the physical fiber element were used to capture the local-buckling induced softening of the I-shaped section column. The simulated results by the physical fiber element fairly agreed with those of the CFEM-shell element. The time-history response calculated by the in-house program using the physical fiber element demonstrated the local buckling-softening had effect on the seismic response.

7. References

[1] Suita, K, Yamada, S, Tada, M, Kasai, K, Matsuoka, Y, Shimada, Y. (2008): Collapse experiment on 4-story steel moment frame: part 2 detail of collapse behavior. *14th World Conference on Earthquake Engineering*, Beijing, China.

[2] Lignos, DG, Krawinkler, H, Whittaker, AS. (2011): Prediction and validation of sidesway collapse of two scale models of a 4-story steel moment frame. *Earthquake. Engng. Struct. Dyn.*, 40, 807–825.

[3] ASCE. (2016) : Minimum design loads for buildings and other structures. *ASCE/SEI-7*. Reston, VA.

[4] Lignos, DG, Krawinkler, H. (2011): Deterioration modeling of steel components in support of collapse prediction of steel moment frames under earthquake loading. *J. Struct. Eng. ASCE*, **137**(11), 1291–1302.

[5] Scott, MH, Fenves, GL. (2006): Plastic hinge integration methods for force-based beam-column elements. *J. Struct. Eng. ASCE*, **132**(2), 244-252.

[6] Uriz, P, Filippou, FC, Mahin, SA. (2008): Model for cyclic inelastic buckling of steel braces. *J. Struct. Eng. ASCE*, **134**(5), 619-628.

[7] D'Aniello, M, La Manna Ambrosino, G, Portioli, F, Landolfo, R. (2013): Modelling aspects of the seismic response of steel concentric braced frames. *Steel and Composite Structures*, **15**(5), 539–566.

[8] Takeuchi, T., Matsui, R, Nagaji, S, Morishita, K. (2015): Elasto-plastic buckling model of H-section steel columns subjected to cyclic bending moment under high axial force. *J. Struct. Constr. Eng., AIJ*, **81**(728), 1723-1732. DOI: 10.3130/aijs.81.1723 (in Japanese)

[9] Kato, B, Fukuchi, Y. (1968): Flange local buckling in plastic range. *Trasnactions of AIJ*, (147), 19-25,71. DOI: 10.3130/aijsaxx.147.0_19 (in Japanese)

[10] Shibata, M, Wakabayashi, M. (1982): Mathematical expression of hysteretic behavior of braces. Part 1 Derivation of hysteresis functions. *Trasnactions of AIJ*, (320), 29-35. DOI: 10.3130/aijsaxx.320.0_29 (in Japanese)

[11] Shimizu, D, Koetaka, Y, Mukaide, S. (2018): Plastic deformation demand of single-story steel frames with braces, *J. Struct. Constr. Eng., AIJ*, **83**(748), 891-901. DOI: 10.3130/aijs.83.891 (in Japanese)

[12] Kato, B, Akiyama, H. (1977): Restoring force characteristics of steel frames equipped with diagonal bracing. Transactions of AIJ, (320), 99-108. DOI: 10.3130/aijsaxx.260.0_99 (in Japanese)

[13] Taniguchi, H, Kato, B, Nakamura, N, Takahashi, Y, Saeki, T, Hirotani, T, Aikawa, Y (1991): Study on restoring force characteristics of X-shaped braced steel frames. *J. of Struct. Eng., AIJ*, **37B**, 303-316. (in Japanese)

[14] Ito, T, Sugiyama, S, Inoue, S. (2015): Restoring force characteristics model considering deterioration behavior of steel compression members subjected to cyclic loading, *J. Struct. Constr. Eng., AIJ*, **80**(710), 715-725. DOI: 10.3130/aijs.80.715 (in Japanese)

[15] Hashimoto, S, Matsui, R, Takeuchi T. (2017): Post-buckling hysteresis and cumulative plastic deformation capacity of concentric steel braces. *JSSC Symposium*, **25**, 825-832. (in Japanese)

[16] Idota, H, Nakata, H, Yoshida, T, Ono, T. (2015): A hysteretic model of laterally supported H-shaped steel beams under cyclic loading, *J. Struct. Constr. Eng., AIJ*, **80**(711), 819-829. DOI: 10.3130/aijs.80.819 (in Japanese)

[17] Matsui, R, Ariga, J, Morishita, K, Kato, M, Takeuchi, T (2019): Collapse analysis of plane frames using phenomenological fiber model of wide flange steel columns, *J. Struct. Constr. Eng., AIJ*, **84**(761), 973-982. DOI: 10.3130/aijs.84.973 (in Japanese)

[18] Takeuchi T, Matsui R. (2015): Cumulative deformation capacity of steel braces under various cyclic loading histories, *J. Struct. Eng.*, **141**. DOI: 10.1061/(ASCE)ST.1943-541X.0001146

